

Wrinkled flames and geometrical stretchBruno Denet^{1,*} and Guy Joulin^{2,†}¹*Institut de Recherche sur les Phénomènes Hors d'Equilibre, UMR 6594 du CNRS, Technopole de Château Gombert, 49 rue Joliot-Curie, 13384 Marseille Cedex 13, France*²*Institut P-prime, UPR 3346 du CNRS, ENSMA, Université de Poitiers, 1 rue Clément Ader, Boîte Postale 40109, 86961 Futuroscope Cedex, Poitiers, France*

(Received 20 December 2010; revised manuscript received 13 April 2011; published 28 July 2011)

Localized wrinkles of thin premixed flames subject to hydrodynamic instability and geometrical stretch of uniform intensity (S) are studied. A stretch-affected nonlinear and nonlocal equation, derived from an inhomogeneous Michelson-Sivashinsky equation, is used as a starting point, and pole decompositions are used as a tool. Analytical and numerical descriptions of isolated (centered or multicrested) wrinkles with steady shapes (in a frame) and various amplitudes are provided; their number increases rapidly with $1/S > 0$. A large constant $S > 0$ weakens or suppresses all localized wrinkles (the larger the wrinkles, the easier the suppression), whereas $S < 0$ strengthens them; oscillations of S further restrict their existence domain. Self-similar evolutions of unstable many-crested patterns are obtained. A link between stretch, nonlinearity, and instability with the cutoff size of the wrinkles in turbulent flames is suggested. Open problems are evoked.

DOI: [10.1103/PhysRevE.84.016315](https://doi.org/10.1103/PhysRevE.84.016315)

PACS number(s): 47.20.-k, 47.32.-y

I. INTRODUCTION

Being of chemical and diffusive origins, flame fronts propagating in premixed gases are markedly subsonic. Thus, because the fresh (ρ_u) and the burnt ($\rho_b < \rho_u$) gas densities differ, flame deformations almost instantly modify the piecewise-incompressible surrounding flow, and vice versa. This *nonlocal* hydrodynamic flame-flow feedback brings about the Darrieus-Landau (DL) [1,2] wrinkling instability, and greatly complicates the free-boundary (hence nonlinear) dynamical flame-front problems, especially from a theoretical viewpoint.

In the limit of small Atwood numbers $0 < \mathcal{A} = (\rho_u - \rho_b)/(\rho_u + \rho_b) \ll 1$, the DL instability is weak, though. Sivashinsky's seminal work [3] showed how flat-on-average flames propagating into a quiescent premixture then evolve according to a nonlocal nonlinear partial differential equation (PDE); subsequent works [4] essentially improved \mathcal{A} -dependent coefficients therein.

Michelson's numerical early study [5] of the PDE showed that unforced flame fronts soon acquire the shape of parabola-like arches joined by sharper crests pointing toward the burnt gas; at late times, a single steady arch (or half-one) with a maximum wavelength compatible with periodic (or Neumann) boundary conditions generically survives in (not-too-wide) channels.

Further numerical investigations [6] of this (Michelson-) Sivashinsky (MS) PDE, exploiting the pole-decomposition method [7], evidenced a much richer manifold of steady solutions whose number increases with available lateral size noticeably faster than linearly. Most of those happen to be unstable and cannot be evidenced by more conventional time-marching procedures.

It would be nice to understand whether a simple mechanism underlies such a proliferation of steady solutions, which has

so far not been done. The present analyses suggest that a *geometrical stretch* (S) induced at large enough scale by a front curvature of the proper sign can noticeably contribute: it indeed generates new couplings with the mechanisms already at work in the MS equation, and generates novel solutions that are steady in a suitable frame. Though unstable, these may play a nontrivial role, like the long-lived weakly unstable states of flat-on-average flames forced by weak noise [6]; or as building blocks of the traveling bursts that are randomly "emitted" near troughs of wide flames [8]. Hence a side question is as follows: is it a spontaneous emission?

A related problem of great practical importance is to understand how velocity modulations or fluctuations in the incoming flow of fresh gas, e.g., time-dependent or even turbulent ones, affect the front dynamics. The problem is unfortunately much too difficult for a frontal theoretical attack. Flames could conceivably be passively deformed at high intensities of forcing, but even the statistics of this is not yet fully understood theoretically [9]. Moreover, the inner cutoff length of front wrinkles in turbulent flows is experimentally known [10] to coincide with the neutral wavelength at which DL instability and curvature effects balance, strongly indicating that the smallest detectable flame wrinkles are not passive.

This hint of forcing-instability interaction at the cutoff length motivates another question: how do incoming velocity *modulations* affect instability-driven patterns at or about such scales?

The point is conceptually different from that of *implantations* of incipient wrinkles by the *small-scale* components of a forcing; these are indeed often present, purposely or because most numerical integration methods are noisy. Despite early attempts about passive forced propagations [11,12], the related mechanism of complex singularity implantation is not understood; unfortunately, it ultimately has a strong impact on flame dynamics [13]. Pole-sprinkling [14] mimics implantations and somehow bypasses the problem, but, although tried for expanding flames [15], this trick is still hampered by its computational cost. To study space- or angle-periodic forced

*bruno.denet@irphe.univ-mrs.fr

†guy.joulin@lcd.ensma.fr

fronts, pseudospectral integration remains more flexible and faster [16].

The present work has a more modest scope: it focuses on *already implanted* patterns and examines their long-term viability in the presence of a *geometrical stretch* caused by an underlying curved front, itself possibly influenced by *large-scale* incoming velocity modulations.

The paper is organized as follows. An extended MS equation accounting for geometrical stretch is introduced in Sec. II. Pole-decomposed steady solutions (in an a frame) are presented in Sec. III, and specialized to a simple centered crest and then to ones with larger amplitudes. The predictions are compared to numerical results in Sec. IV. Multicrested “steady” wrinkles are identified and analyzed in Sec. V, and their self-similar unsteady counterparts are discussed in Sec. VI. Section VII takes up varying S 's. Section VIII tentatively relates the cutoff scale of wrinkling to stretch, and Sec. IX gathers final remarks and open problems. Appendixes A and B detail technical points.

II. NONLINEAR EQUATION FOR STRETCHED ISOLATED WRINKLES

The starting point adopted here to take up the aforementioned topics is a nondimensional forced version of the (Michelson-)Sivashinsky [3] PDE:

$$\phi_t + \frac{1}{2}\phi_x^2 = \nu\phi_{xx} + I(\phi, x) + u(t, x). \quad (2.1)$$

It governs the shape $y = \varphi(t, x)$ of a flame observed in the frame (x, y) of a flat one ($\varphi \equiv 0$) propagating toward the fresh gases ($y < 0$) at the laminar flame speed u_L . The subscripts t (time) and x (abscissa) stand for partial derivatives, and the linear *nonlocal* operator $I(\varphi, x)$, defined by $I(e^{ikx}, x) = |k|e^{ikx}$, accounts for the hydrodynamic DL instability that affects premixed flames at long wavelengths. The scaled Markstein length [17] $\nu > 0$, proportional to the actual flame-front thickness ℓ based on u_L and the fresh-gas heat diffusivity, measures how the local burning speed u_n of a flame element relative to fresh gases responds to curvature, $u_n - u_L \sim \nu\phi_{xx}$.

With $u(t, x) = 0$, the linearized Eq. (2.1) admits normal modes $\varphi \sim \exp(ikx + \varpi t)$ whose growth or decay rate is $\varpi(k) = |k|(1 - \nu|k|)$. In the present units [$\sim \mathcal{A}^{-2}\ell/u_L$ for time, $\sim \ell/\mathcal{A}$ for abscissa and Markstein length, $\sim \ell$ for wrinkle amplitude, and $\sim \mathcal{A}^2 u_L$ for speed variations], the range of unstable wave numbers and the shortest growth time are $0 \leq |k| \leq k_n = 1/\nu$ and $1/\varpi(k_n/2) = 4\nu$, respectively. The “eikonal” term $\varphi_x^2/2$ in (2.1) results from the secant of the small angle $\alpha(t, x)$ between local (normal to the front) and mean (y -axis) directions of propagation, $(1 + s^2)^{1/2} - 1 = s^2/2 + \dots$, $s = \tan(\alpha) \sim \mathcal{A}\varphi_x$. The stabilizing effect of $\varphi_x^2/2$ can saturate the DL instability [5], soon leading to parabola-like arches when $u(t, x) = 0$.

The forcing term u in Eq. (2.1) represents the y -wise component of a shear-flow type of modulation in the fresh-gas flow; $u(t, x) \neq 0$ may also result from an inhomogeneous and/or fluctuating fresh gas composition that makes u_n change [18]. Without its DL contribution $I(\varphi, x)$, Eq. (2.1) would be an inhomogeneous Burgers equation modeling *passive* propagations.

Let $\Phi(t, x)$ represent a solution of Eq. (2.1). Another one, $\varphi(t, x)$, is sought in the form $\varphi = \Phi + \phi$, where $\phi(t, x)$ represents extra wrinkles grown on top of the base flame shape Φ . The “excess” function $\phi(t, x)$ satisfies the homogeneous equation

$$\phi_t + \Phi_x \phi_x + \frac{1}{2}\phi_x^2 = \nu\phi_{xx} + I(\phi, x), \quad (2.2)$$

where the multiplicative Φ_x accounts for the *geometry* of the base solution of Eq. (2.1), and hence is partly tributary to the forcing function in (2.1), especially if it is large. In fact, the structure of (2.1) indicates how to select $u(t, x)$ to yield (almost) any presumed $\Phi(t, x)$.

We next assume that, possibly helped by a proper choice of the forcing function, one may approximate the base pattern $\Phi(x, t)$ by a parabola over the region where a localized ϕ_x “lives.” With $\Phi_x \approx Sx + U$, Eq. (2.2) acquires the simpler, yet still nonlocal and nonlinear, form

$$\phi_t + (Sx + U)\phi_x + \frac{1}{2}\phi_x^2 = \nu\phi_{xx} + I(\phi, x), \quad (2.3)$$

first proposed as a model with $U = 0$ and briefly studied in [19]. Whatever the value of U is, Eq. (2.3) admits infinitesimal solutions $\phi = A(t) \exp\{iq(t)[x - \chi(t)]\}$, provided the wave-number $q(t)$, amplitude $A(t) \ll \lambda(t) = 2\pi/q$, and shift $\chi(t)$ satisfy $dq/dt = -Sq$, $dA/dt = A\varpi(q)$, $d\chi/dt = U$. So, while the disturbance drifts, a positive $S > 0$ *stretches* its wavelength, $\lambda(t) \sim \exp[\int_0^t S(t')dt']$; $S < 0$ is often termed “compression.” $U(t)$ can be formally removed by a change of coordinate [$x - \chi(t)$ used instead of x] and is henceforth omitted. Yet it must be kept in mind that *the “steady” patterns encountered later will only be so in a specific frame drifting at the uniform lateral speed U* . A locally uniform x -wise gas velocity $v(t, 0)$ and the associated $v(t, 0)\phi_x$ could have been accounted for in Eq. (2.3) and then lumped in U and “eliminated,” but the S -dependent term cannot. The curvature S of the base pattern Φ is here termed “stretch intensity.” Incidentally, an $Sx\phi_x$ term appears when studying self-similar rational solutions to the Burgers equation [20]; $x = X/E$ is then an abscissa measured in a t -dependent unit of length $E(t)$.

III. CENTERED STEADY PATTERNS

Attention will be focused hereafter on *finite-amplitude* solutions to Eq. (2.3), namely *localized* patterns ϕ that are peaked near the origin and have ϕ_x^2 and $I(\phi, x)$ decaying like $(\nu/x)^2$ at large distances; the DL term $I(\phi, x)$ is then $\int_{-\infty}^{+\infty} \phi_x/(x - x')\pi dx'$. Time-independent S 's, as exist about the troughs (wide local minima) of steady base-flame profiles Φ when unforced [21], are considered first (t -dependent ones will be touched upon in Sec. VII). Localized solutions to the nonlinear (2.3), e.g., the steady ones (in a suitable frame) considered below, bring about a continuum of Fourier modes, which makes them difficult to handle numerically by spectral methods. The pole-decomposition technique recalled below bypasses the difficulty.

A. Pole equations

As first shown in [7,22], the MS PDE [Eq. (2.3) with $U = 0 = S$] admits exact nonperiodic solutions ϕ representing localized patterns that are “steady” and have

$$\phi_x = \sum_{n=-N}^N \frac{-2\nu}{x - iB_n}. \quad (3.1)$$

The iB_n 's, with $B_n > 0$ for $n=1,2,\dots,N$ and $B_{-n} = -B_n$ (ϕ is real when x is), are poles of the flame slope ϕ_x continued in the complex z plane, $z = x + iB$. These carry the same “charge” (residue) -2ν , fixed by the dominant balance $\phi_x^2/2 \sim \nu\phi_{xx}$ near each $z = iB_n$. Equation (3.1) was shown in [19] to also hold when $S \neq 0$. When t -independent, such B_n 's, $|n| = 1, \dots, N$, obey

$$\sum_{n \neq m = -N}^N \frac{2\nu}{B_n - B_m} - \text{sgn}(B_n) + SB_n = 0, \quad (3.2)$$

where the $\text{sgn}(\cdot)$ function results from the DL instability [$1/(x - iB)$ has $-i\text{sgn}(B)/(x - iB)$ as a Hilbert transform]; the sum comes from nonlinearity and SB_n from stretch. Since $B_{-n} = -B_n$, summing Eq. (3.2) over $n \geq 1$ yields $B_{\text{bar}} - SB_{\text{rms}}^2 \equiv \nu(2N - 1)$; this “sum rule” exactly relates the barycenter (or center of mass) $B_{\text{bar}} \equiv (B_1 + \dots + B_N)/N$ of the positive B 's to their variance $B_{\text{rms}}^2 \equiv (B_1^2 + \dots + B_N^2)/N$, a useful check of accuracy for numerical resolutions.

B. Elementary centered steady crest

The case of one pole pair [$N = 1, \phi_x - iI(\phi, x) = -4\nu/(x - iB_1), B_1 > 0$], corresponding to an elementary steady wrinkle centered at $x = 0$, is particularly simple as (3.2) gives a quadratic:

$$\nu/B_1 - 1 + SB_1 = 0. \quad (3.3)$$

A single real solution $B_1 \leq \nu$ is found for $S \leq 0$ (compression), but two of them exist if $0 \leq S < S_c \equiv 1/4\nu, \nu \leq B^- \leq B^+$, with B^- (or B^+) going to ν (or $+\infty$) as $S\nu \rightarrow 0^+$. Two “steady” elementary crests are then admissible, that with $B_1 = B^-$ being sharper and narrower. If $0 < S\nu \ll 1$, the B^- root essentially results from a balance between DL instability and nonlinearity, $1 \approx \nu/B^-$; B^+ is then of a different type mainly governed by the DL effect and stretch, $1 \approx SB^+$. Both branches $B^\pm(\nu, S)$ merge at $B_c = 2B^-(\nu, 0) = 2\nu$ when S coincides with the dimensionless maximum growth rate, $S_c = \varpi(k_n/2)$ (see Sec. II); $2S_c B_c = 1$ then holds. No steady solution with a single pair of poles $\pm iB_1$ is allowed if $S > S_c$. The generalization of Eq. (3.3) to t -dependent B 's (Sec. IV) reveals that the B^+ root is unstable, and that $S > S_c$ leads to $B_1(t/\nu \rightarrow \infty)/\nu = \infty$, i.e., wrinkle suppression.

Importantly, the DL instability is a necessity of this stretch-induced crest suppression, needed as it is to balance two stabilizing effects [see (3.3)]: one is only intense at short scale (nonlinearity) and the other at large distance (stretch), and the balance is impossible if $S > S_c$.

C. Large centered steady crests

In the stretch-free case, the uppermost pole altitude increases with the number N of pole pairs, and the typical

difference $B_n - B_{n-1}$ becomes small compared to $B_{\text{max}} = \max(B_n)$ if $N \gg 1$; one may then replace the discrete sum featured in Eq. (3.2) by an integral over a continuous measure [7], such that $P(B)dB$ is the number of imaginary poles iB with “altitudes” between B and $B + dB$. When applied to Eq. (3.2), the continuous approximation leads to an integral equation for the density $P(B) = P(-B)$:

$$\int_{-B_{\text{max}}}^{+B_{\text{max}}} \frac{2\nu P(B')dB'}{B - B'} = \text{sgn}(B) - SB, \quad (3.4)$$

where the principal-part integral complies with the constraint $m \neq n$ in Eq. (3.2). Although (3.4) formally is the difference between its $S = 0$ version and a Wigner equation [no $\text{sgn}(B)$ on the right-hand side [23]], one may not subtract partial solutions: (3.4) does not hold for $|B| > B_{\text{max}}$, where no pole lies, and B_{max} itself must be found as part of the complete solution, thanks to the overall normalization $\int_0^{B_{\text{max}}} P(B')dB' = N$.

Equation (3.4) is solved by a Fourier method as in [21] (see Appendix A). In terms of an angle, $-\pi/2 \leq \theta \leq +\pi/2$ defined by $B = B_{\text{max}} \sin \theta$, $P(B)$ reads

$$2\pi^2\nu P(|B| \leq B_{\text{max}}) = \ln[\cot^2(\theta/2)] - \pi SB_{\text{max}} \cos \theta, \quad (3.5)$$

and $P(|B| \geq B_{\text{max}}) = 0$. With $\sin \theta = B/B_{\text{max}}$ and $2\nu P(B)$ fixed by Eq. (3.5), a contour integration in the θ plane (or p. 591 of [24]) expresses $\phi_x = -\int_{-B_{\text{max}}}^{+B_{\text{max}}} 2\nu P(B')dB'/(x - iB')$ in terms of $\sinh \xi \equiv x/B_{\text{max}}$ as $\text{sgn}(-x)\pi\phi_x = \ln[\coth^2(\xi/2)] - SB_{\text{max}} \cosh \xi$. The ensuing crest profile reads $\text{sgn}(x)\pi\phi(x)/B_{\text{max}} = -\sinh \xi \ln[\coth^2(\xi/2)] - 2\xi + SB_{\text{max}}(\xi + \sinh \xi \cosh \xi)/2$, up to an additive constant. The large steady crest thus has $[\phi(x) - \phi(0)]/B_{\text{max}} = F(|x|/B_{\text{max}}, SB_{\text{max}})$, and is ν -independent. The cumulative pole distribution $R(B) \equiv \int_0^B P(B')dB'$ deduced from (3.5) is

$$2\pi^2\nu R(B)/B_{\text{max}} = \sin \theta \ln[\cot^2(\theta/2)] + 2\theta - SB_{\text{max}}(\theta + \sin \theta \cos \theta)/2, \quad (3.6)$$

to be compared with $i\pi\phi(ix)$. The corresponding center of mass of positive B 's, $B_{\text{bar}} \approx \int_0^{B_{\text{max}}} P(B')B'dB'/N$, has $\pi B_{\text{bar}}/B_{\text{max}} = (1 - w/3)/(1 - w/4)$, $w \equiv \pi SB_{\text{max}}$, and can be notably less than the yet unknown B_{max} ; the “shape factor” $B_{\text{rms}}/B_{\text{bar}}$ also varies weakly with w .

Finally, the normalization of $P(B)$ rewritten as $R(\theta = \pi/2) = N$ completes the resolution of Eq. (3.4). It relates B_{max} and νN to the stretch intensity S by an analog of (3.3):

$$(2\pi N\nu)/B_{\text{max}} - 1 + (\pi S/4)B_{\text{max}} = 0, \quad (3.7)$$

the structure of which again parallels (3.2) and the “sum rule” [expressed as $(2N - 1)\nu/B_{\text{bar}} - 1 + (B_{\text{rms}}^2/B_{\text{bar}}^2)SB_{\text{bar}} = 0$].

A single large crest again exists at fixed $N\nu$ regardless of $S \leq 0$, and has $B_{\text{max}} \leq 2\pi\nu N$. Just like with (3.3), two values B^\pm of B_{max} [hence two densities $P^-(B), P^+(B)$] are obtained for $0 \leq S \leq S^*$, namely $2\pi\nu N \leq B^-(\nu N, S) \leq B^*$ and $B^+(\nu N, S) \geq B^*$ with

$$S^* \equiv 1/(2\pi^2 N\nu), \quad B^* \equiv 4\pi N\nu. \quad (3.8)$$

Similar to the two-pole case, both branches merge at $B^* = 2B^-(\nu N, 0)$ when $S = S^*$. No real B_{max} exists if $S > S^*$, and the DL mechanism [middle term of (3.7)] again is needed for

crest suppression. And *larger wrinkles are easier to suppress*: $\nu S^* \sim 1/N$.

Put differently, a given stretch intensity $0 < S\nu \ll 1$ allows for a large centered steady crest iff $1 \ll N \leq N^* \equiv \lfloor 1/2\pi^2\nu S \rfloor$ ($\lfloor \cdot \rfloor \equiv$ integer-part). In case the number of pole pairs exceeds N^* initially, at least $N - N^*$ of them will ultimately be expelled to $|B| \gg N\nu$ as time elapses (see below for the pole dynamics): *the stretch intensity selects the width and amplitude of the surviving crest; both scale like the radius of curvature $1/S$ of the base flame in any case*: $2S^*B^* = 4/\pi \approx 1.27$ for $N \gg 1$, $2S_c B_c = 1.00$ for $N = 1$.

IV. NUMERICAL VERSUS ANALYTICAL

Two numerical approaches were employed to study Eq. (3.2): (i) use Newton-type iterations, which are delicate to initiate in case of multiple solutions yet give access to stable and unstable ones, and can benefit from analytically determined seeds; (ii) acknowledge that Eq. (3.2) are the restriction to steady and pure imaginary poles iB_n of more general equations [7,19] for the poles $z_j(t) = x_j(t) + iB_j(t)$ of ϕ_x in unsteady situations, viz.

$$\frac{dz_j}{dt} = \sum_{-N, q \neq j}^{+N} \frac{2\nu}{z_q - z_j} - i \operatorname{sgn}[\operatorname{Im}(z_j)] + Sz_j, \quad (4.1)$$

where $\operatorname{Im}(\cdot)$ denotes an imaginary part; the front slope $\phi_x(t, x)$ then is a sum, similar to Eq. (3.1), of $-2\nu/[x - z_j(t)]$ contributions. Each pole pair constitutes a soliton and, as the dynamics (4.1) conserves their number N (if finite), the pole-decomposition method is noise-free. Numerically integrating Eq. (4.1) only yields stable equilibria at large times, but gives access to stability properties of any steady solution already at hand (t may be run backward).

When restricted to $z_j = iB_j$, the numerical procedure(s) always led to an equilibrium if $N < N^*$ and the pole imaginary parts initially have $|B| < B^+$. The numerical pole density P_{num} , defined by $P_{\text{num}}[(B_j + B_{j-1})/2] \equiv 1/(B_j - B_{j-1})$ and linear interpolation in between, is compared with the predictions (3.5) and (3.7) in Fig. 1 for $1/\nu = 199.5$, $N = 100$, $S = 0.05 \approx S^*/2$, showing excellent agreement up to $B = (B_N + B_{N-1})/2$; this also holds for the corresponding cumulative density $R(B)$ along the lower branch [i.e., with $B_{\text{max}} = B^-(\nu N, S)$ in Eq. (3.5)], again not too close to $|B| = B_{\text{max}}$, a point that will be commented on at the end of this section.

Still, in no way could one obtain a density $P_{\text{num}}(B)$ resembling Eq. (3.5) if used with $B_{\text{max}} = B^+(\nu N, S)$, even when $B^+(\nu N, S)$ and $B^-(\nu N, S)$ have comparable magnitudes. This relates to an additional constraint, not visible in (3.4) and (3.7): pole densities must be non-negative. For $|B| \approx B_{\text{max}}$, the analytical prediction (3.5) has $2\pi^2\nu P(B) \approx (2 - \pi S B_{\text{max}}) \cos \theta$, which gets negative indeed at $|B| \lesssim B_{\text{max}}$ if $S B_{\text{max}} > 2/\pi = S^* B^*$; see Eq. (3.7). Thus, even though our starting assumptions $N \gg 1$ and $S < S^*$ are fulfilled, the upper branch $B_{\text{max}} = B^+(\nu N, S) > S^* B^*/S$ and the corresponding profile $\phi(x)$ are *spurious*.

Instead of $P^+(B)$, the density $P_{\text{num}}(B)$ obtained by Newton-Raphson iterations with N pole pairs and $S < S^*$ approached the prediction (3.5) if used with $B_{\text{max}} = B^-(\nu N, S)$; or, de-

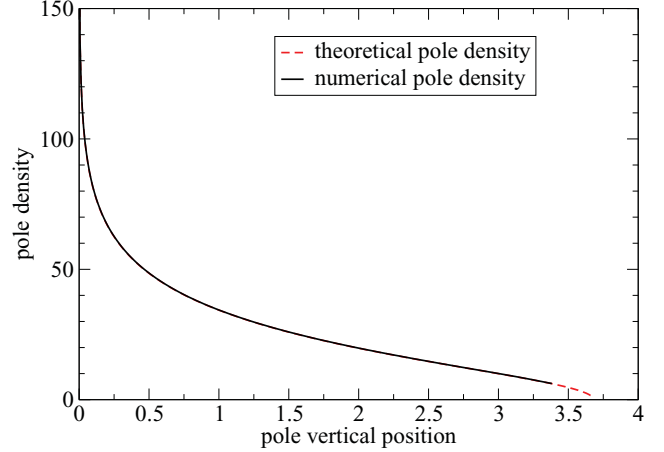


FIG. 1. (Color online) Numerical pole density $P_{\text{num}}(B)$ vs pole altitude B (solid black) compared to the analytical prediction $P^-(B)$, Eqs. (3.5) and (3.7), with $B_{\text{max}} = B^-(\nu N, S)$ (dashed red). Both curves have $1/\nu = 199.5$, $N = 100$ ($S^* = 0.102 \dots$), and $S = 0.05$.

pending on the initial B 's used as iteration seeds, the converged density $P_{\text{num}}(B)$ happened to be close to that corresponding to $B^-(\nu(N-1), S)$ but supplemented with a single pair of remote poles $\pm ih$, with $h \approx 1/S - \nu(4N-3) + \dots$ for $0 < S\nu \ll 1$. The latter estimate results from a balance (at $B = h$) between stretch, the DL effect, and the combined vertical repulsions from the complex conjugate (located at $B = -h$) and from the $2(N-1)$ other poles considered positioned at their barycenter ($B = 0$):

$$1 - Sh \approx \nu/h + 4\nu(N-1)/h, \quad 0 < S\nu \ll 1, \quad (4.2)$$

to be compared with (3.3). A more complete determination of h accounts for the full pole distribution with density $P^-(B)$ spread over $[-B_{\text{max}}, +B_{\text{max}}]$, instead of a mere global charge $4\nu(N-1)$ positioned at $B = 0$. Once the integrals over $P^-(B)dB$ are analytically evaluated (see pp. 591 and 393 of [24]), the equation for h looks like (4.2), except for its last term, which is replaced by $(2/\pi) \arcsin(B_{\text{max}}/h) - S B_{\text{max}}^2 / (h + (h^2 - B_{\text{max}}^2)^{1/2})$, with $B_{\text{max}} = B^-(\nu(N-1), S)$. This resumes the form (4.2) when $S\nu \ll 1$ and provides one with a useful test of the numerical method and convenient seeds for iterations: for $S = 0.01$, $\nu = 0.1$, and $N = 4$, the more complete expression gives $h = 98.682\,569$ while the exact (numerical) value is $98.682\,595$. The ‘‘center of charge’’ estimate (4.2) gives $98.682\,645$ and is still a few percent accurate up to nearly $S = S^*$; this accuracy is to be used in Sec. VI.

Interestingly, the existence of a detached pole pair in equilibrium signals the appearance of a *new type of crest structures* that bifurcate from $|B| = \infty$ at $S = 0^+$, in a sense generalizing the B^+ root of Sec. III [Eqs. (4.2) and (3.3) coincide if $N = 1$]. More general arrangements involving several remote poles will be encountered in Secs. V B and VI B.

Solving Eq. (3.2) iteratively for different stretch intensities with a fairly large N ($=100$) and $\nu \approx 1/2N$ gives the relationship between S and the upper barycenter B_{bar} shown in Fig. 2; the modification of $B_{\text{bar}}(\nu N, S)$ caused by the existence of a detached pair of remote poles $\pm ih$ is also

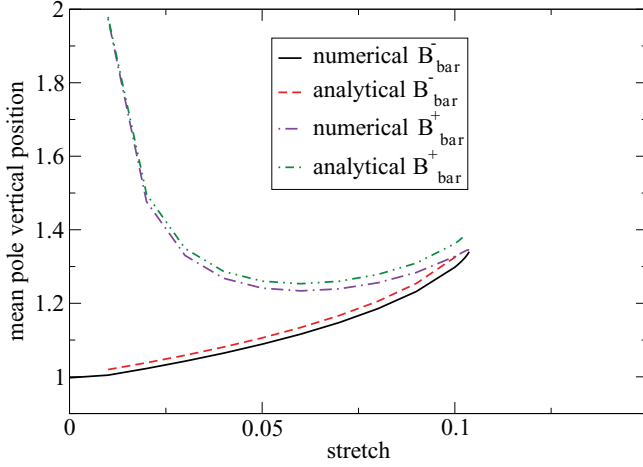


FIG. 2. (Color online) Barycenters of $N = 100$ pole pairs aligned along the imaginary axis vs stretch intensity S for $1/\nu = 199.5$ [$S^* = 0.102 \dots$, Eq. (3.8)], without detached poles (lower curves) or with them (upper curves). Solid (black) and dash-dotted (violet) lines: Newton-Raphson iterations from the steady Eq. (4.1); dashed (red) and dash-double-dotted (green) lines: analytical predictions; see text.

plotted and compared to the theoretical estimate $B_{\text{bar}}^+ = (1 - 1/N)B_{\text{bar}}(\nu(N - 1), S) + h/N$. As expected from Eq. (3.7), the existence of a maximum admissible stretch intensity S^* [hence of a maximum admissible number N^* of aligned poles at fixed $S > 0$] is numerically confirmed for large centered crests as well. However, while displaying similar trends to the corresponding numerical B_{bar} and B_{bar}^+ , both analytical predictions systematically exceed them by a visible amount that slowly increases with S (and N). This, in fact, results from a failure of the continuous approximation wherever the density $P^-(B)$ gets too small, i.e., at $|B| \lesssim B_{\text{max}}$. As shown in [7,21], good estimates of the *discrete* pole locations $B_j > 0$ can be retrieved from the continuous cumulative distribution $R(B)$ on solving $R(B_j) = j - 1/2$, $j = 1, \dots, N$, but this deteriorates at $|B_j| \lesssim B_{\text{max}}$. As for the extreme zeros of Hermite polynomials at large degrees [25], the region where $R(B)$ ceases to correctly count the pole labels has a size that may be estimated by $0 < R(B_{\text{max}}) - R(B_N) \sim 1$. With $N - R(B) \lesssim B_{\text{max}}$ deduced from (3.6), this results in $B_N = B_{\text{max}}\{1 - [g(\pi S B_{\text{max}})/N]^{2/3}\}$, $g(w) \sim (1 - w/4)/(1 - w/2) > 0$. Thus, $B_{\text{max}}/B_N - 1 > 0$ decays with $1/N$ and increases with S (yet rather slowly), but $B_{\text{max}} - B_N \sim \nu[g(w)N]^{1/3}$ grows with N and S : there is no numerical flaw in Figs. 1 and 2. Overestimating B_N as B_{max} in turn shifts B_{bar} and B_{bar}^+ by about the same fractional amount.

V. A VARIETY OF STEADY LOCALIZED PATTERNS

The previous centered isolated crests are unstable to lateral shifts. Writing the pole locations as $z_j(t) = D(t) + Z_j(t)$ leaves Eq. (4.1) invariant if $D(t) = D(0)\exp(St)$, whereby a steady crest pattern can be dragged as a whole by a geometry-induced tangential velocity $\Phi_x \approx Sx$, away from the base flame trough $x = 0$. Besides, [7] identified the reason why a population of nearby poles tends to align along parallels to the imaginary z axis (see also [20]) and to build up a crest.

This results from a “horizontal” attraction encoded in the pairwise interaction terms of Eq. (4.1), combined with the “vertical” repulsion featured in Eq. (3.2). If $|z_q - z_j| \ll B_{\text{max}}$, $d(z_q - z_j)/dt \approx -4\nu/(z_q - z_j)$, whereby $\text{Im}(z_q - z_j) \text{Re}(z_q - z_j) \approx \text{const}$: $|\text{Re}(z_q - z_j)|$ decays during the near collision, while $|\text{Im}(z_q - z_j)|$ grows; this short-range alignment mechanism still operates with a nonzero S [incidentally, it would still act at short distance in the presence of an extra damping in (2.2), say $\sim \phi$, but not at large scale].

A. Nearly real crests or poles

One may thus conceive that steady twin crests might stay in equilibrium “at” $x = \pm X_1$ ($X_1 > 0$) under two antagonistic actions: “repulsive” lateral convection SX ($S > 0$) and the horizontal attraction felt by each crest’s pole, $+X_1 + ib_n$ say, caused by the $2N_1$ poles $-X_1 + ib_m$ belonging to the crest’s twin. Balancing the two effects gives $X_1 \sim (2N_1\nu/S)^{1/2}$: if $S\nu N_1 \ll 1$, the pole-pole height $B_{\text{max}} \sim 2N_1\nu$ is small compared to crest spacing $2X_1$ (as presumed), a situation henceforth referred to as “nearly real” crests (or pole) arrangements.

For $N_1 \gg 1$, $\nu N_1 = O(1)$, and any S , the poles of a steady symmetric two-crest pattern are not exactly aligned vertically but actually reside along two disjoint *curves*, $z(b) = x(b) + ib$ and $-x(b) + ib$, with $0 < x(b) = x(-b)$ and $|b| < b_{\text{max}}$. Both curves share the pole density $p(b) = p(-b)$ per unit length along the b axis, with $\int_0^{b_{\text{max}}} p(b)db = N_1$ for normalization, and the real unknowns $x(b)$ and $p(b)$ obey a *complex-valued* generalization of (3.4) deduced from (3.2):

$$\int_{-b_{\text{max}}}^{+b_{\text{max}}} \frac{2\nu p(b')db'}{z(b) - z(b')} = Sz(b) - isgn(b) - \int_{-b_{\text{max}}}^{+b_{\text{max}}} \frac{2\nu p(b')db'}{z(b) + z(b')}. \quad (5.1)$$

Only for small stretch intensities, $0 < S\nu N_1 \ll 1$, could we solve (5.1) analytically for $z(b)$: to two orders in S all the poles are found to remain aligned at $\pm X_1 \pm ib + o(1)$, with $X_1 \gg b = O(\nu N_1)$ now defined by $SX_1 \equiv (2N_1 \times 2\nu)/(2X_1)$. Their density $p(b)$ still obeys (3.4) with $\{p(b), N_1\}$ in lieu of $\{P(B), N\}$, but with S replaced by $S + S/2$ as the $z(b)$ are not exactly real. The large-scale influence they feel from the other distant crest is not quite uniform, yet it may be Taylor-expanded for $|b| \ll 2X_1$ to produce a linear term $(z - X_1)(2N_1)(2\nu)/(2X_1)^2 = (z - X_1)S/2$ that ultimately contributes the extra $S/2$. As a net consequence, the results for isolated crests, e.g., those encoded in Eqs. (3.5) and (3.7) for $N \gg 1$, still hold for twin crests once $0 < S \ll 1/\nu N_1$ is replaced by $3S/2$; this replacement is required whatever the value of N_1 is. If $0 < S\nu N_1$ takes on $O(1)$ values, the vertical pole alignments deform, with $|x(b)|$ decreasing faster at smaller $|b|$.

Multicrested steady solutions also are unstable against shifts $[\sim \exp(St)]$ as a whole. They then provide one with localized burstlike disturbances, akin to those invoked by Zel’dovich *et al.* [26] but here of *finite* amplitudes, *traveling along the nearly parabolic base flame front* $Sx^2/2$; Fig. 3 shows a sample traveling burst comprising eight poles. These bursts admittedly are also unstable with respect to

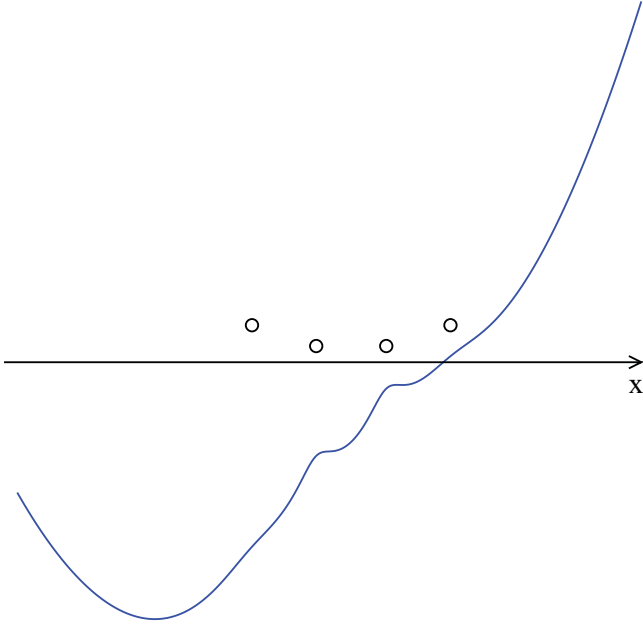


FIG. 3. (Color online) Solid (blue) line: Snapshot of a finite-amplitude, four-pole-pair lateral “burst” $\phi(t, x)$ superimposed to the base shape $Sx^2/2$ ($S = 1, \nu = 1/10, N = 4$). The four pole locations in the upper $x + iB$ plane are shown as open circles above the x axis. The scale is identical in all directions.

modifications of the crest mutual distances, yet the presence of several nearby crests may help some survive longer as a result of the “horizontal” interactions: to wit, a many-crested pattern may be steady if properly centered [in the frame evoked below (2.3)].

One might indeed have assumed that the previously considered isolated crest centered at $x = X_0 = 0$, with its N_0 pairs of poles $iB_{0,n}$, still is present: a steady three-crest pattern is thus conceivable, with the lateral ones (again with N_1 pole pairs each) staying at a distance $\pm X_1$ given by $SX_1 = (2N_0)(2\nu)/X_1 + (2N_1)(2\nu)/(2X_1)$ if $0 < \nu SN_{0,1} \ll 1$. The construction may be pursued with five crests peaked at the abscissas $0 = X_0, \pm X_1, \pm X_2$, or four crests at $\pm X_1, \pm X_2$, etc.

More generally, let M be the number of crests involved in a steady arrangement and N_k the number of pole pairs belonging to the k th crest. This kind of configuration will henceforth be referred to as an $(N_1, \dots, N_k, \dots, N_M)$ solution, and, whenever needed, the superscript “+” (e.g., N_k^+) will indicate that a pair of poles is separated from the considered pole pile as $S\nu N_k \rightarrow 0+$. For $S > 0$ small enough that the typical crest spacing [anticipated to be $\sim (N_k \nu S)^{1/2}$] noticeably exceeds $(B_{\max})_k \sim \nu N_k$, the crest abscissas X_k must satisfy the conditions of equilibrium of M “charges” $4\nu N_k$, $k = 1, \dots, M$, subject to attractive horizontal $1/X$ interactions, and all sit on a common quadratic potential barrier $-SX^2/2$,

$$-\sum_{j=1, j \neq k}^M \frac{4\nu N_j}{X_k - X_j} + SX_k = 0. \quad (5.2)$$

Apart from the condition $N_1 X_1 + \dots + N_M X_M = 0$, which necessarily holds, the above crest number M and weights N_k are only constrained by $1 \leq M \leq N_{\text{tot}} \equiv$

$N_1 + \dots + N_M$. As a result, the combinatorial explosion makes the number $\mathcal{N}(N_{\text{tot}})$ of such conceivable “stretch versus nonlinearity” nearly real equilibria rapidly grow with N_{tot} . The function $\mathcal{N}(N_{\text{tot}})$ grows faster than the number ($\sim \exp[\pi(2N_{\text{tot}}/3)^{1/2}]/N_{\text{tot}}$ for $N_{\text{tot}} \gg 1$ [27]) of unordered integer partitions of N_{tot} because unequal weights N_k may be permuted; yet \mathcal{N} grows less rapidly than that ($= 2^{(N_{\text{tot}}-1)}$ [28]) of ordered partitions because $x \leftrightarrow -x$ mirror images of admissible asymmetric patterns also exist, which leads to double-counting: since most patterns are asymmetric, we conjecture that $\mathcal{N}(N_{\text{tot}}) \approx 2^{(N_{\text{tot}}-2)} \gg N_{\text{tot}}$ different patterns with near-real poles exist for $N_{\text{tot}} \gg 1$. At any rate, the above combinatorial reasoning suggests that *weak positive stretch allows for a proliferation of steady solutions*.

Only in the two particular instances evoked as follows could Eq. (5.2) be solved analytically with unequal weights N_k . The first situation has only two crests of arbitrary weights N_- and N_+ located at $X_- < 0 < X_+$. Equation (5.2) readily yields $X_{\pm} = \pm 2N_{\mp}[\nu/S(N_+ + N_-)]^{1/2}$. A Taylor expansion like below (5.1), here for $|z - X_{\pm}| \ll X_+ - X_-$, shows that the poles belonging to either crest again receive an extra contribution from their neighbor, besides the imposed $0 < \nu S \ll 1$. Here, this entails the replacements $S \rightarrow S_{\pm} \equiv S[1 + N_{\pm}/(N_+ + N_-) + \dots]$ for the stretch intensity effectively felt by either crest, all poles of which are aligned vertically within $o(\nu N_{\pm})$ errors if $0 < \nu SN_{\pm} \ll 1$ and could thus be analyzed via (3.2) or (3.4); $N_+ = N_-$ clearly yields $S_+ = 3S/2 = S_-$ as below (5.1). The more populated crest feels a greater effective influence of stretch and will be the first to lose remote poles if $S\nu N_{\pm} > 0$ gets too high.

The second situation amenable to some analysis corresponds to a centered crest composed of N_0 vertically aligned pole pairs, symmetrically flanked by $N + N$ lateral crests that have $N_{|k| \geq 1} = N_1$ pole pairs each. The (horizontal) equilibrium of the central crest at $X_0 = 0$ is then guaranteed by symmetry. In the limit $0 < S\nu N_1 \ll 1$, the $N + N$ lateral crest locations $X_k = -X_k$, with $|k| = 1, \dots, N$, obey a particular form of (5.2):

$$\sum_{-N=j \neq k, 0}^{j=N} \frac{4\nu N_1}{X_k - X_j} + 4\nu \frac{N_0}{X_k} = SX_k. \quad (5.3)$$

Its solutions can be expressed as $X_k = \text{sgn}(k)(4\nu N_1 \eta_{|k|}/S)^{1/2}$ in terms of the zeros $\eta_{|k|} > 0$ of the associated Laguerre polynomial $\mathcal{L}_N^{(\alpha)}(\eta)$ of degree N and order $\alpha = N_0/N_1 - 1/2$; this follows from Stieltjes’ classical analysis of electrostatic problems [29] (see Appendix B).

For $N_0 = 0$ or $N_0 = N_1$, the X_k ’s are actually zeros of the M th-order Hermite polynomial, $\mathcal{H}_M[X_k(S/4N_1\nu)^{1/2}] = 0$, with $M = 2N$ or $2N + 1$, since $\mathcal{H}_{2N}(\xi^2) \sim \mathcal{L}_N^{(-1/2)}(\xi^2)$ and $\mathcal{H}_{2N+1}(\xi) \sim \xi \mathcal{L}_N^{(+1/2)}(\xi^2)$ ([24], p. 1001). Numerical resolutions of (4.1) in this case reveal that the “Hermite” approximation is excellent if $S\nu N_1 \ll 1$, but Table I shows it still works fairly well even for stretch intensities S comparable to the value (again noted S^*) at the turning point.

Table II shows similar results corresponding to $2N + 1 = 7$, with $N_0 = 3$ pairs for the central crest and $N_1 = 1$ for the lateral ones: the fuller “Laguerre” approximation, still excellent at small $S\nu > 0$, again locates the crests fairly

TABLE I. Numerically determined abscissas $X_k > 0$ of crests with “near-real” poles versus those estimated from the Hermite polynomial, $\mathcal{H}_M[X_k(S/4N_1\nu)^{1/2}] = 0$, for $N_k = N_1 = 1$, $M = 7$, $\nu = 1/10$ (this solution’s turning point is at $S^* \approx 0.55$), and $S = 0.25$. As when $S\nu N_1 \ll 1$, all numerical poles have $|\text{Im}(z_k)| \approx \nu$.

$ k $	Numerical X_k ’s	Hermite X_k ’s
1	1.0281177	1.03253157
2	2.1081804	2.11689397
3	3.3416002	3.35449526

accurately for S ’s comparable to the value S^* at the turning point. Increasing the stretch intensity beyond S^* makes a pole pair separate from the central pile, reducing its weight. For $0 < \nu S N_{0,1} \ll 1$, the effective stretch intensity felt by the central crest is $S_0 = S(1 + 1/\eta_1 + \dots + 1/\eta_N + \dots)$; as shown in Appendix B, S_0 also reads $S[1 + 2N/(N_0/N_1 + 1/2) + \dots]$ and may exceed the maximum stretch intensity that an isolated crest of weight N_0 can resist, $S^* \approx 1/(2\pi^2 N_0 \nu)$ for $N_0 \gg 1$, even if $\nu N_1 S \ll 1$.

Thus, the antagonistic actions of horizontal attraction between nearby crests and geometry-induced positive stretch near *any* flame trough (e.g., that of the base solution Φ we started from) generates new equilibrium positions: other poles may sit there if the effective stretch intensity they feel is compatible with a vertical equilibrium, making secondary troughs appear on the flame profile, and so forth. This gives hints on how the *stretch-nonlinearity competition is sufficient to contribute a complicated web of steady solutions to the MS equation* [6]. As shown below, still more exotic configurations exist for almost the same reason.

B. Remote poles

In the above equilibria, between “almost real” pole pairs in the presence of a weak enough stretch effect, Eq. (5.2), the DL instability mechanism has only a slight direct influence on the crest spacing, merely ensuring that nearly real poles remain so. Similar configurations could conceivably exist when the members of N poles pairs are markedly off the real axis, provided these lie at nearly the same altitudes $\pm ih$; an elementary configuration of this type (a single detached pair) was encountered in Sec. IV. The height $h > 0$ has to significantly exceed x_{\max} for this to be viable: the repulsive influence that each of the N poles $\approx x_k \pm ih$ inside one single row feels from the complex conjugates (now at a distance of $2h$) must indeed be nearly uniform and weak enough not

TABLE II. Comparison between the numerically determined abscissas X_k of $2N = 6$ crests with “near-real” poles ($N_1 = 1$ pole pair each) in the presence of a central crest comprising $N_0 = 3$ pole pairs and those $[X_k = \text{sgn}(k)(4\nu N_1 \eta_{|k|}/S)^{1/2}]$ estimated from the roots of the Laguerre polynomial $\mathcal{L}_N^{(\alpha=3/2)}(\eta)$ for $\nu = 1/10$ (turning point at $S^* \approx 0.12$) and $S = 0.06$.

$ k $	Numerical X_k ’s	Laguerre X_k ’s
1	3.4237352	3.48790272
2	5.6222914	5.6649485
3	8.0750858	8.10819913

to destroy the possibility of a “DL versus stretch” balance with $0 < S\nu \ll 1$. For $h \gg x_{\max}$, the “vertical” equilibrium requires

$$1 - Sh = 2\nu N/2h + \dots \quad (5.4)$$

at the two leading orders [compare to Eqs. (3.3) and (4.2)], whereby $h = 1/S - \nu N + \dots$ will self-consistently exceed $x_{\max} \sim (\nu N/S)^{1/2}$ when $0 < S\nu \ll 1$. As for the “horizontal” equilibria among the remote poles located at $z \approx x_k \pm ih$, one can show that their abscissas x_k ’s satisfy

$$-\sum_{0=j \neq k}^{j=N} \frac{2\nu}{x_k - x_j} + Sx_k = 0, \quad k = 1, \dots, N \quad (5.5)$$

to leading order for small positive S ’s. The Stieltjes analysis [29,30] implies the x_k ’s are again given by roots of a Hermite polynomial in first approximation, yet with a scale different from the nearly real cases: $\mathcal{H}_N[x_k(S/2\nu)^{1/2}] = 0$; since the largest zero of \mathcal{H}_N is $O(N^{1/2})$ regardless of $N \geq 1$, $x_{\max} \sim (\nu N/S)^{1/2} \ll 1/S$ if $N \ll 1/\nu S$, as guessed. Though *a priori* limited to small stretch intensities (it is then excellent), this calculation evidences that *steady remote pole arrangements of a novel type exist when $0 < S\nu \ll 1$* . Used with $B_k = \pm i(1/S - \nu N)$ and $\mathcal{H}_N[x_k(S/2\nu)^{1/2}] = 0$ as seeds for the pole locations, Newton-Raphson numerical resolutions of the steady Eq. (4.1) reveal that such remote arrangements survive for noninfinitesimal stretch intensities in a range, and show that the numerical x_k lie near the roots of Hermite polynomials even when their altitudes $|\text{Im}(z_k)| \approx h$ are not large compared to x_{\max} any longer; see Table III.

Comparisons of the above near-horizontal remote pole arrangements with Refs. [6,31] suggest that a similar stretch-based mechanism underlies the “interpolating solutions” of the MS equation evidenced there, where approximately horizontal arrangements of poles are found to lie at a distance above and between the vertically aligned ones pertaining to the main crests; the stretch is then due to the main crest curvature Φ_{xx} and, ultimately, results from the attraction by the array of vertically aligned poles belonging to the space-periodic base front slope Φ_x (instead of the pole-at-infinity of Sz in the present situation).

As if that is not enough, for some given sets $\{S, \nu, N_{\text{tot}}\}$ either type of pole arrangement (all close to the real axis or near the altitudes $\pm h \gg \nu N_k$) can be obtained, depending on the initial seed chosen in Newton iterations; each type may have its own turning point, at least when N is moderate.

TABLE III. Comparison between the numerically determined abscissas $x_k > 0$ of horizontally aligned “remote” poles $\pm x_k \pm ih$ with those estimated from the Hermite polynomial $\mathcal{H}_N[x_k(S/2\nu)^{1/2}] = 0$ for $N_1 = 7$, $\nu = 1/10$, and $S = 0.30$; the turning point is at $S^* \approx 0.69$, and numerics gives $|\text{Im}(z_k)| \approx 2.53$ only.

$ k $	Numerical x_k ’s	Hermite x_k ’s
1	0.71748382	0.66649627
2	1.4684599	1.36644918
3	2.3196838	2.16531738

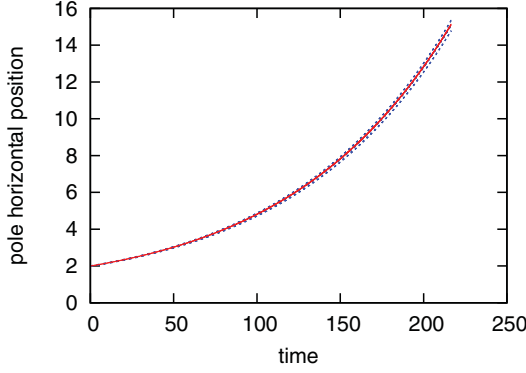


FIG. 5. (Color online) Dotted (blue) lines: Evolutions of the scaled abscissas $X_k(t)/L_{\text{eq}}^0 \xi_k > 0$ of 3 (out of $M = 7$) nearly real crests initially at about $X_k(0)/L_{\text{eq}}^0 \xi_k = 2$ (twice the equilibrium values), for $S = 1/100$, $\nu = 1/10$, $N_{k \geq 1} = N_1 = 1$, and purposely disturbed initial poles locations (see text). Solid (red) line: analytical prediction, Eq. (6.3).

imaginary part of (4.1), their current common altitude $h(t) \gg O[(N\nu/S)^{1/2}]$ must obey

$$dh/dt = N\nu/h - 1 + Sh + \dots \quad (6.7)$$

instead of (5.4), whereas the unsteady version of (5.5) (dx_k/dt is added to the right-hand side) has solutions $x_k(t) = L(t)\xi_k + D(t)$ still given by (6.2), (6.3), and (6.6), up to a few differences.

(i) First, one must set $N_k = N_1 = 1$ in (6.2) and (6.5), whereby the equilibrium scale factor is now $L_{\text{eq}}^\infty \equiv (2\nu N/S)^{1/2}$. Yet like previously, *steady nearly horizontal remote pole arrangements are unstable*: $|L| \sim \exp(St)$ for $St \gg 1$ if $|L(0)| > L_{\text{eq}}^\infty$, whereas $|L(0)| < L_{\text{eq}}^\infty$ leads to the collapse of all (simple) poles into a single one (of order

N) at the finite $t = t_{\text{merger}}$, $St_{\text{merger}} \equiv -\ln[1 - [L(0)/L_{\text{eq}}^\infty]^2]$. (ii) Another difference with near-real poles is that the dynamics (6.5) does not stop at $t = t_{\text{merger}}$. $L^2(t)$, as is now defined by (6.6), may get negative and $L(t)$ itself imaginary: the N poles then become *vertically* aligned, and will remain nearly so for $t > t_{\text{merger}}$.

The latter scenario of course assumes that the altitude $h(t)$ has not shrunk to zero in the interim: whereas $h(0) > h_{\text{eq}} = 1/S - \nu N + \dots$ eventually leads to $h \sim \exp(St)$ and poles that head for $\pm i\infty$, any $h(0) < h_{\text{eq}}$ will drive the solution of (6.7) to $h(t_0) = O[(N\nu/S)^{1/2}] \ll 1/S$ for $t \approx t_0$, $St_0 \equiv -\ln[1 - h(0)/h_{\text{eq}}]$; after t_0 the poles in question will shortly become nearly real, $h(t > t_0) = O(\nu) \ll (N\nu/S)^{1/2}$. The analysis just given then ceases to be valid, but the previous one pertaining to nearly real pole pairs becomes applicable: at $t \approx t_0$ the poles are indeed separated by $O[(N\nu/S)^{1/2}]$ horizontal distances, and in a first approximation for $0 < SN\nu \ll 1$ their abscissas are still proportional to the zeros ξ_k of a Hermite polynomial, $\mathcal{H}_N(\xi)$. If $t_0 < t_{\text{merger}}$, i.e., $h(0)/h_{\text{eq}} < [L(0)/L_{\text{eq}}^\infty]^2$, and such that $L(t_0) < L_{\text{eq}}^0$ [or $L(t_0) > L_{\text{eq}}^0$], an N -crest pattern will be seen to crop on top of the base flame before collapsing into a single one (or an N -crest pattern expanding laterally); on the contrary, if $t_0 > t_{\text{merger}}$, only an isolated crest will be observed when acquiring a significant amplitude.

Thus, depending on the values of the initial altitude $h(0)$ and scale factor $L(0)$, a variety of behaviors caused by nonlinear interactions may take place among initially remote pole arrangements, even though this can hardly be noticed from the real axis because the poles involved are too far from it when these “off-stage” processes occur. Moreover, slight differences in the initial conditions may result in completely different patterns as time elapses: *the unstable equilibria* [e.g., remote poles at $\xi_k L_{\text{eq}}^\infty \pm ih_{\text{eq}}$, or near-real ones at $\xi_k L_{\text{eq}}^0 \pm iO(\nu N_k)$] *play the part of “shunting” or “saddle” points for the system trajectories*. Since the poles are indiscernible (identical residues), the existence of unstable equilibria, whose number quickly increases as $1/S\nu \rightarrow +\infty$, almost precludes one from tracing back the origin of subwrinkles of a weakly curved flame front from the sole observation of their shape, location, and amplitude when they become visible. This likely contributes to the nearly random manner in which subwrinkles crop up on top of weakly curved flame troughs [8], like in a Galton box.

VII. TIME-DEPENDENT STRETCH

A too intense constant stretch $S > 0$, for example induced by a too strong steady $u(x)$ in Eq. (2.1), can moderate or inhibit the phenomenon of trough-splitting (i.e., crest formation) that the DL instability mechanism tends to induce. On the contrary, a constant compression, $S < 0$, tends to pull the poles of ϕ_x and to make them crowd near the origin $z = 0$. What happens when S oscillates and possibly changes sign with time has so far not been investigated, even though this relates to the subwrinkles of flames subjected to a time-dependent, nonuniform $u(t, x)$ in Eq. (2.1). Oscillating stretch intensities $S(t) = \langle S \rangle + \sigma \sin(\omega t)$ of various mean values $\langle S \rangle$, amplitudes σ , and frequencies ω are considered below.

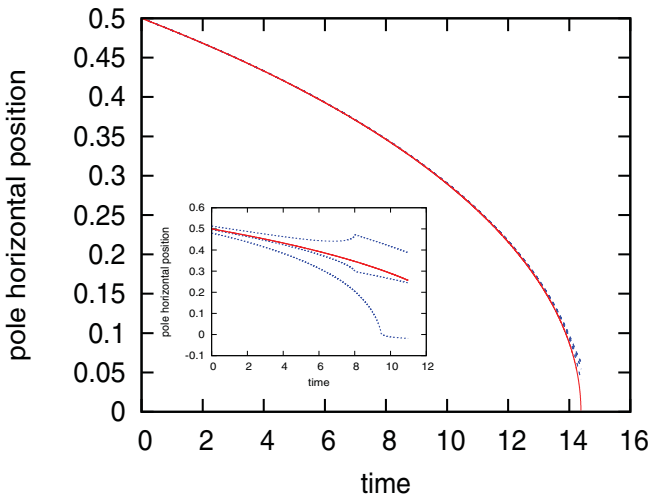


FIG. 6. (Color online) Dotted (blue) lines: Evolution of the scaled abscissas $X_k(t)/L_{\text{eq}}^0 \xi_k > 0$ of 3 (out of $M = 7$) near-real crests initially at $X_k(0)/L_{\text{eq}}^0 \xi_k = 1/2$ (half the equilibrium values) for $S = 1/100$, $\nu = 1/10$, $N_{k \geq 1} = N_1 = 1$. Solid (red) curves: analytical prediction, Eq. (6.3). Inset: as previously, with the same intentional “noise” on initial conditions as in Fig. 5.

At frequencies $\omega \ll 1/\nu$, the quasisteady approximation applies, whereby a slowly evolving two-pole centered crest may not be durably viable whenever $\max(S) = \langle S \rangle + \sigma$ exceeds $S_c = 1/4\nu$; see Sec. III A. Its quasisteady structure will cease to exist when $S(t)$ crosses S_c for the first time: even if $S(t)$ may later cross S_c from above, $B_1(t)$ will have meanwhile moved high enough above the unstable $B^+(\nu, S(t))$ not to again be attracted near the lower branch $B^-(\nu, S(t))$ of quasisteady solutions. Likewise, centered crests with $2N \gg 1$ vertically aligned poles are ruled out whenever $\langle S \rangle + \sigma$ exceeds S^* for long enough, Eq. (3.8), but can nevertheless survive with a smaller number of pole pairs, $N \leq \lfloor 1/2\pi^2\nu(\langle S \rangle + \sigma) \rfloor$ (see Sec. III B). In other words, *at least when it is slow, the $S(t)$ history selects N in the long-time limit.*

To study the opposite, high-frequency, case $\omega \gg 1/\nu$, one first sets $B_n = \beta_n E(T)$, $E \equiv \exp[-(\sigma/\omega) \cos T]$, $T = \omega t$, and next invokes a two-time (t and T) asymptotic method, formally replacing d/dt by $\omega d_T + \partial_t$. Provided they remain $O(N\nu)$ to leading order for $\omega \gg 1/\nu$, the $\beta_n(t, T)$ functions may actually only depend on the “slow” time t ; taking an average (noted $\langle \cdot \rangle$) of (4.1) over T shows they obey the “slow dynamics,”

$$\frac{\partial \beta_n}{\partial t} = \sum_{-N=m \neq n}^{m=N} \frac{2\nu K}{\beta_n - \beta_m} - J \operatorname{sgn}(\beta_n) + \langle S \rangle \beta_n. \quad (7.1)$$

Here $a \equiv \sigma/\omega$, $J \equiv \langle \exp[\pm a \cos(\omega t)] \rangle = I_0(a)$, with $I_0(\cdot)$ being the modified Bessel function of the first kind and zeroth order, and $K \equiv I_0(2a)$. This averaged dynamics for the β_n 's thus has the same structure as the restriction of (4.1) to aligned poles $z_n = iB_n$, up to coefficients that only depend on (σ/ω) , i.e., on the power spectrum of the integrated stretch fluctuations.

In particular, the late time state of a two-pole ($N = 1$) oscillating crest must satisfy $\nu K/\beta_1 - J + \langle S \rangle \beta_1 = 0$ instead of (3.3), and will be allowed only if $\langle S \rangle$ is less than $\langle S \rangle_c$, with

$$\langle S \rangle_c = S_c J^2/K < S_c, \quad (7.2)$$

where $S_c = 1/4\nu$ is the same as in the nonoscillating, two-pole case; see (3.3). The corresponding value of β_1 is $2\nu K/J > B_c = 2\nu$, and that of $\langle B_1 \rangle$ is even larger, $\langle B_1 \rangle = 2\nu K$, not to mention $\max[B_1(t)] = \beta_1^\pm \exp(a) > \nu K \exp(a)$. In other words, an intense enough high-frequency oscillating component of the stretch intensity tends to flatten a two-pole crest [$\langle \beta_1 \rangle > B^-$ along the lower branch β_1^- of steady solutions to (7.1)]: more importantly, fast enough *oscillations in stretch intensity make subwrinkle suppression easier than by the mean stretch alone*, $S_c \geq \langle S \rangle_c$, yet moderately so since J^2/K only slowly decays from $1 - a^2/2 + \dots$ at $|a| \ll 1$ to $\approx 1/(\pi|a|)^{1/2}$ at $|a| \gg 1$. One may also note that $2\langle S \rangle_c \langle B \rangle_c = J > 1$, indicating a weaker and wider crest profile at the turning point than without fluctuations of stretch intensity.

The numerical integration of (4.1) with $N = 2$, $\nu = 1/10$, $\omega = 20$, and $a = 3/2$ ($J^2/K = 0.555\dots$) shows that a successful two-time analysis does not require ω to largely exceed the reciprocal relaxation time t_1 of $\beta_1(t)$ to the steady root β_1 : in Fig. 7, $\omega t_1 \approx 3.5$. The large- ω predictions tend to be more accurate for the highest poles.

Likewise, crests with $N \gg 1$ aligned pole pairs subjected to high-frequency stretch are ultimately described by an equation similar to (3.4), yet with $\{\nu, S\}$ replaced by $\{\nu K/J, \langle S \rangle/J\}$.

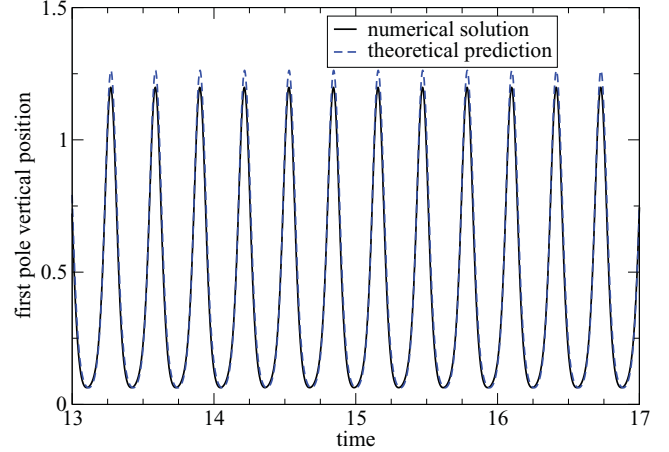


FIG. 7. (Color online) Black solid line: oscillating solution $B_1^-(t)$ obtained from numerical integration of Eq. (4.1) for $N = 2$ ($z_k = iB_k, |k| = 1, 2$) for $\nu = 1/10$, $S(t) = 0.2 + 30 \sin(20t)$. Dashed (blue) line: analytical curve $\beta_1 \exp[-(\sigma/\omega) \cos T]$, $\beta_{1,2}$ being the positive steady solutions of (7.1).

They may therefore exist only if $2\pi^2 N \nu \langle S \rangle < J^2/K < 1$: again, the condition for stretch-induced crest suppression is more restrictive than (3.8). In the large- ω limit, the instantaneous crest slope has $E(T)\phi_x = -\int_0^{+\beta_{\max}} 4\nu X p(\beta) d\beta / (X^2 + \beta^2)$, with $X \equiv x/E(t)$, and the equations that determine the $p(\beta)$ have the same structure as (3.4) provided $\{\nu, S, B, B_{\max}\}$ are replaced therein by $\{\nu K/J, \langle S \rangle/J, \beta, \beta_{\max} = \langle B_{\max} \rangle/J\}$; the corresponding instantaneous crest shape is ultimately self-similar, $\phi(t, x) = F(X)$.

Before closing this section, a few remarks are in order. The large- ω analysis can be easily adapted when the fluctuation $S'(t)$ of stretch intensity contains R widely separated frequencies $1/\nu \ll \omega_1 \ll \omega_2 \ll \dots \ll \omega_R$, with partial amplitudes σ_r : the influence of each frequency can be accounted for in turn, starting from ω_R . As a result, the J coefficient involved in the slowest dynamics (7.1) becomes $J = I_0(a_1)I_0(a_2) \cdots I_0(a_R)$, $a_r \equiv \sigma_r/\omega_r$, and K acquires a similar expression. Because $\ln[I_0(|a| \ll 1)] = a^2/4 + \dots$, such products converge for $R = \infty$ whenever the power spectrum of the integrated stretch fluctuation satisfies the comparatively mild condition $\sigma_r/\omega_r = o(1/r^{1/2})$. Whereas also allowing $\langle S \rangle$ to depend on slow time t is a harmless additional generalization, it is not known whether the above elementary “cascade renormalization” [32] can be extended to a continuous spectrum $\omega \geq \omega_1 \gg 1$ (replacing the series for $\ln J$ and $\ln K$ by integrals over $\omega \geq \omega_1$), and to turbulent-like fluctuations of S ; the analogs of J and K could even be tabulated numerically if $S'(t) = S(t) - \langle S \rangle$ is available and contains no beat with $\omega\nu = O(1)$.

At any rate, the convexity of exponential functions guarantees that $\langle E \rangle \geq 1$, $\langle E^2 \rangle \geq 1$ for any $d(\ln E)/dt = S'(t)$ such that the latter time averages exist. The Cauchy-Schwartz inequality implies $J^2/K = \langle E \rangle^2 / \langle E^2 \rangle \leq 1$, whereby *the trends revealed with harmonic variations of stretch intensity are fairly general*. They actually extend to fronts that are $2\pi E(t)/\kappa$ -periodic ($\kappa > 0$) in x , in which case $S'(t) = d(\ln E)/dt$. This pertains to $x \rightarrow -x$ invariant flame fronts propagating along the center line (y -axis) of left-right symmetric

two-dimensional channels with a variable width $\Lambda(y) > 0$ [33]. The scale factor is then $E(t) = \Lambda(\hat{t}u_L)/\langle\Lambda\rangle$, $\hat{t} \sim t\ell/u_L\mathcal{A}^2$ being a dimensioned time, whereby $\langle S \rangle = 0$ and $\langle E \rangle = 1$; the analog of J/K again is less than 1. One can show that the number N of pole pairs present “in” the channel must be less than $\lfloor(1 + J/\nu\kappa K)/2\rfloor$ if a cellular pattern is to survive; this is more stringent than when $\Lambda(y) \equiv \langle\Lambda\rangle$ (i.e., $J = K$), and no wrinkle is allowed durably in the wavy channel if $J/K \leq \kappa\nu$.

VIII. STRETCH VERSUS SPECTRAL CUTOFF

To put the findings obtained so far in a more physical perspective, and relate them to the second problem evoked in Sec. I, it is useful to restore dimensions in the “stretched” MS equation (2.3). This gives

$$\hat{\phi}_t + a(\mathcal{A})u_L[\Sigma\hat{x}\hat{\phi}_x + \frac{1}{2}(\hat{\phi}_x)^2] = u_L\Omega(\mathcal{A})[\hat{\phi}_{xx}/k_n + I(\hat{\phi}, \hat{x})], \quad (8.1)$$

where the overhats of \hat{x}, \hat{t}, \dots denote dimensioned variables, and the uniform drift velocity $\hat{U}(\hat{t}) \sim U(t)$ is again omitted: $\hat{\Phi} \equiv \Sigma\hat{x}^2/2$ represents the parabolic background front, on top of which subwrinkles of local amplitude $\hat{\phi}(\hat{t}, \hat{x})$ grow. The dimensionless grouping $a(\mathcal{A}) \approx (1 + \mathcal{A})$ and the DL coefficient $0 \leq \Omega(\mathcal{A}) \approx [(1 + \mathcal{A})/(1 - \mathcal{A})]^{1/2} - 1$ only depend on the Atwood number $0 < \mathcal{A} = (\rho_u - \rho_b)/(\rho_u + \rho_b) < 1$, and are known from separate analyses [1–4].

The “ultimate” steady subwrinkle (in the proper frame) that can survive as the stretch intensity $u_L\Sigma$ (now a reciprocal time) increases is the *two*-pole solution at its turning point [the same as at $S = S_c = 1/4\nu$ in (3.3)]; see Figs 5 and 9. It corresponds to a total (i.e., base-flame + subwrinkle) dimensioned flame profile $\hat{\phi} \equiv \hat{\Phi} + \hat{\phi}$ of the form

$$\hat{\phi}_c = \frac{\Omega(\mathcal{A})}{a(\mathcal{A})k_n}\psi(\hat{x}k_n), \quad \psi(\xi) \equiv \frac{\xi^2}{8} - 2\ln\left(1 + \frac{\xi^2}{4}\right). \quad (8.2)$$

The function $(3/4 - \ln 4)[1 - \cos(\pi\xi/\sqrt{12})]$ accurately osculates $\psi(\xi)$ at and between its min or max, located at $\xi = 0, \pm\sqrt{12}$; see Fig. 8. This suggests that, as a result of

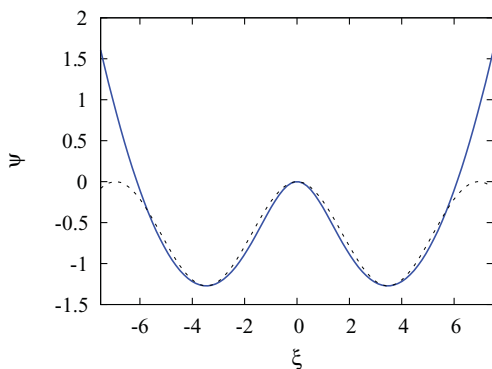


FIG. 8. (Color online) Solid (blue) curve: total flame-front shape at turning point $\Sigma = \Sigma_{\text{cutoff}}$ of the two-pole crest, $\psi(\xi) \equiv \xi^2/8 - 2\ln(1 + \xi^2/4)$, vs $\xi = \hat{x}k_n$. Dashed (black) line: osculating cosine [see below Eq. (8.2)].

the geometrical stretch caused by distortions at larger scale, *it is unlikely that visible wrinkles with wave numbers $|k| \geq k_{\text{cutoff}} = (\pi/2\sqrt{3})k_n \approx 0.9k_n$ exist*, provided the local wrinkle structure is considered to be quasisteady. Since the crest radii of curvature essentially scales like $1/k_n$ regardless of their amplitude [7], this result is compatible with the experimentally known near-equality between neutral and cutoff wave numbers for the wrinkle spectrum of flames propagating in turbulent flows.

This result $k_{\text{cutoff}} \approx k_n$ is not a mere dimensional consequence of having the Markstein length \mathcal{L} as a reference in problems of flame dynamics, since $k_n\mathcal{L}$ depends on the Atwood number: to wit, $k_n\mathcal{L} \approx \Omega(\mathcal{A}) \sim \mathcal{A}$ for $\mathcal{A} \ll 1$. Next, the condition for suppression of all steady subwrinkles by geometrical stretch ($S > S_c$ in the notation of Sec. III) can be rewritten as $\mathcal{D} > \mathcal{D}_c \equiv 1/a$, where \mathcal{D} is a Damköhler number [34]. It is defined as the ratio of the rate-of-strain $u_L\Sigma$ based on flat-flame speed u_L and the background flame curvature Σ [a tributary of the forcing function in (2.1)] to the maximum DL growth rate $\Omega(\mathcal{A})u_Lk_n$; this suggests a dynamical origin. That *a balance of nonlinearity, DL instability, and stretch is a necessity of wrinkle suppression* [see (3.3)] confirms the genuine *flame-dynamical origin* of the $\mathcal{D} > \mathcal{D}_c$ criterion, and the presence of $a(\mathcal{A})$ [weight of nonlinearity in (8.1)] in \mathcal{D}_c further substantiates this.

The unsteadiness caused by a time-dependent Σ will admittedly bring about numerical factors [e.g., the grouping J^2/K in (7.2)] in the above criterion; yet those will stay $O(1)$ unless $u_L\Sigma(\hat{t})$ and the frequencies ω it involves are much higher than, $O[u_L\Omega(\mathcal{A})k_n]$. That, however, is unlikely for turbulent flames propagating through actual reactive gaseous premixtures in conditions when a thin front of $O(\ell)$ thickness can be identified as such, because this requires $u_L\Sigma(\hat{t})$ and ω to be much smaller than u_L/ℓ [34], and $\Omega(\mathcal{A}) = O(1)$ in practice: the estimate $k_{\text{cutoff}} = O(k_n)$ is then expected to still hold true in such regimes, which it does [10,35].

As shown in Sec. III, the approximate result $2S \max(B) \approx 1$ was obtained at turning points regardless of the number N of pole pairs involved, thereby suggesting that $O(1/\Sigma)$ typical wrinkle size (amplitude and width) could be selected by the fluctuating stretch intensity $u_L\Sigma(\hat{t})$, when $\Sigma \ll \Sigma_{\text{cutoff}} \equiv \Omega k_n/4a$. This militates in favor of a (mean-) power spectrum of wrinkling tied to that of stretch intensity at moderately small wave-number ratios k/k_n : the estimate $\hat{B} \approx 1/2\Sigma$ for the typical subwrinkle amplitude \hat{B} prevailing at larger scales than $1/k_{\text{cutoff}}$ might then form the basis of a scaling law of the form $\Sigma^{-1}(k)f(k/k_{\text{cutoff}})$ for the (mean-) power spectrum of wrinkling, with a nearly constant (or very small) $f(\cdot)$ at $k/k_n \ll 1$ (or $k/k_n \gg 1$).

IX. FINAL REMARKS, OPEN PROBLEMS

Combining analytical and numerical approaches based on the pole decomposition, the present work revealed that inclusion of geometrical stretch markedly modifies the otherwise simple [7,19] isolated solutions of the classical (Michelson-) Sivashinsky PDE for (weakly) unstable flames.

First, it was demonstrated that accounting for a uniform stretch intensity S is enough to generate novel types of isolated solutions. New steady (unstable) solutions with arrays of

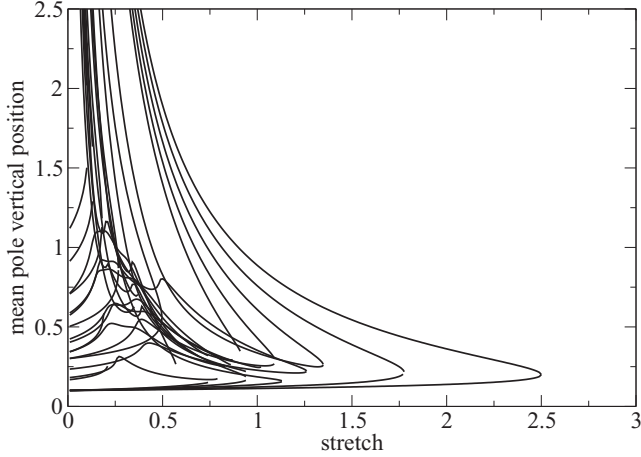


FIG. 9. Compiled B_{bar} (upper-pole barycenter) vs $S \geq 0$ (dimensionless stretch intensity) curves obtained in the present work for $\nu = 1/10$, up to $N = 8$ for some of them. Curves with $N \leq 3$ already appeared in Fig. 4, e.g., the rightmost solution (3.3) ($N = 1$).

horizontally aligned near-real or remote poles (or both) were evidenced; when $S = 0$, only *one* centered isolated solution, involving a single vertical pole alignment, existed regardless of $N \geq 1$ [21].

The net result is a proliferation of equilibrium front shapes, especially at small S 's; see Fig. 9.

Part of the complexity of MS-type equations (even if $S = 0$) boils down to the fact, caused by a nonlinearity and a curvature term already present in the Burgers equation, that the spatial poles of ϕ_x are indiscernible and interact pairwise via a $1/z$ law: midway between two such singularities, another one can stay in equilibrium. A specificity of this nonlinearity-induced phenomenon is the anisotropy (horizontal attraction versus vertical repulsion) of the $1/z = \bar{z}/|z|^2$ law. In contrast, stretch effects act on front singularities (hence on their shape) in an isotropic way. Their presence brings about the possibility of new “stretch versus horizontal attraction” and/or “stretch versus Darrieus-Landau instability” partial equilibria, thereby noticeably contributing to the quick proliferation of (unstable) steady solutions when $S > 0$ decreases. A similar mechanism operates in periodic solutions of the stretch-free MS equation: S is then effectively provided by the curvature of the main cell trough, and the many poles associated with its crests provide the means to pull extra wrinkles or poles away from the trough in a nearly isotropic way. The analogy is further substantiated by the fact that the new stretch-induced “steady” states found above are unstable, as are those evidenced in [6,31]; their self-similar evolution, described analytically, will likely help handle those bursts traveling along wide front troughs.

It has also been shown that too intense stretch suppresses all isolated “steady” wrinkles (Fig. 9); the larger and wider the wrinkles, the easier the suppression: this is not caused by a local quenching of combustion processes inside the front structure [34], but results from an untenable balance between stretch, geometrical nonlinearity, and nonlocal hydrodynamics (and curvature). As the above analyses showed, this effect is only quantitatively modified when the stretch intensity oscillates, crest suppression being just made somewhat easier.

These findings have been used to suggest this mechanism as the reason why the wrinkle upper cutoff wave number in turbulent flames coincides experimentally [10] with the neutral wave number identified by linear stability analyses.

Classical (orthogonal) polynomials were encountered when studying stretch-induced horizontal pole and crest equilibria. This is not unduly surprising because these are not directly affected by the Darrieus-Landau mechanism, and hence they are electrostatic-like. The needed polynomials obey differential *local* equations, yet the classical ones do not cover all “horizontal” equilibria at weak stretch; some available generalizations (e.g., Heine-Stieltjes polynomials [30]) will hopefully do.

But concerning the “vertical” equilibria, the situation is much less clear. The *nonlocal* DL instability mechanism indeed acts on the pole population in a way that is explicitly “vertical,” encoded as it is in an irremovable Hilbert transform. Further studies of the “stretched Sivashinsky polynomials,” whose roots obey the steady pole equations, seem warranted, e.g., to theoretically elucidate the very *nature* of the miracle that allows the MS equation to have pole-decomposed solutions (hidden symmetries or mere good fortune?) and because the Darrieus-Landau mechanism is an indispensable ingredient of stretch-induced wrinkle suppression.

Yet another important theoretical point is dangling. Implicit in the discussion about the influence of stretch on the wrinkle wave number (Sec. VIII) was the assumption that the maximum admissible number of front-slope poles, corresponding to turning-point conditions, is the relevant one: since the pole dynamics conserves their number (when finite), how can noise supply “enough of” them as the stretch intensity varies? This brings one back to a *nonlinear* problem already evoked in Sec. I: how does noise, even if weak when seen on the real axis, implant complex poles (incipient wrinkles)? Answering this question is one of the most challenging open theoretical issues about flame dynamics, not to mention its statistical aspects.

APPENDIX A: THEORETICAL POLE DENSITY

Setting $B = B_{\text{max}} \sin \theta$, $\text{sgn}(B) = \text{sgn}(\theta)$ and $P(B) = P(-B)$ are expanded as Fourier series:

$$\pi \text{sgn}(B) = \sum_{j=0}^{\infty} 4 \sin [(2j+1)\theta]/(2j+1), \quad (\text{A1})$$

$$P(B) = \sum_{j=0}^{\infty} P_j \cos [(2j+1)\theta]. \quad (\text{A2})$$

Employing them and the identity [21]:

$$\int_{-\pi/2}^{+\pi/2} \frac{\cos[(2j+1)\theta'] \cos \theta'}{\sin \theta - \sin \theta'} d\theta' = \pi \sin [(2j+1)\theta], \quad j = 0, 1, \dots \quad (\text{A3})$$

in (3.4) then yields $2\pi\nu P_j = 4/(2j+1) - \pi S B_{\text{max}} \delta_{0j}$ (δ_{0j} = the Kronecker delta); summing the series for $P(B)$ gives Eq. (3.5) of the main text.

APPENDIX B: STIELTJES TRICK FOR CREST LOCATIONS

Multiplying each of Eq. (5.3) by $X_k = -X_{-k}$ and setting $X_k = \text{sgn}(k)(4\nu N_1 \eta_{|k|}/S)^{1/2}$ leads to

$$2\eta_k \sum_{1=j \neq k}^N \frac{1}{\eta_k - \eta_j} + \alpha + 1 - \eta_k = 0, \quad (\text{B1})$$

with $\alpha = N_0/N_1 - 1/2$. As first realized by Stieltjes [29,30], the above sum over $j \neq k$ can also be written as $\lim_{\eta \rightarrow \eta_k} \{p'(\eta)/p(\eta) - 1/(\eta - \eta_k)\} = p''(\eta_k)/2p'(\eta_k)$, where

$p(\eta) \equiv \prod_{k=1}^N (\eta - \eta_k)$ and $(\cdot)' = d(\cdot)/d\eta$. Next, the polynomial $\eta p''(\eta) + (\alpha + 1 - \eta)p'(\eta)$ has $-N\eta^N$ as the term of highest degree; according to the equations above, it vanishes when $\eta = \eta_k, k = 1, \dots, N$, and thus it is $-Np(\eta)$. As the only polynomial solution of $\eta p'' + (\alpha + 1 - \eta)p' + Np = 0$ is an associated Laguerre polynomial, one has $p(\eta) = \mathcal{L}_N^{(\alpha)}(\eta)$ [24], and its accessible roots $\eta_k > 0$ give the crest locations; see Sec. V. The sum $1/\eta_1 + \dots + 1/\eta_N$ of the roots $1/\eta_k$ of $\mathcal{L}_N^{(\alpha)}(\eta)/\eta^N$ is deducible from the known coefficients [24] of $\mathcal{L}_N^{(\alpha)}(\cdot)$, and reads $2N/(\alpha + 1) = 2N/(N_0/N_1 + 1/2)$.

-
- [1] G. Darrieus, work presented at La Technique Moderne, Paris, 1938 (unpublished).
- [2] L. D. Landau, *Acta Physicochim. URSS* **19**, 77 (1944).
- [3] G. I. Sivashinsky, *Acta Astronaut.* **4**, 1177 (1977).
- [4] P. Clavin and G. I. Sivashinsky, *J. Phys. (France)* **48**, 193 (1987).
- [5] D. N. Michelson and G. I. Sivashinsky, *Acta Astronaut.* **4**, 1207 (1977).
- [6] B. Denet, *Phys. Rev. E* **74**, 036303 (2006).
- [7] O. Thual, U. Frisch, and M. Hénon, *J. Phys. (France)* **46**, 1485 (1985).
- [8] D. M. Michelson and G. I. Sivashinsky, *Combust. Flame* **48**, 211 (1982).
- [9] T. Sasamoto and H. Spohn, *J. Stat. Mech.* **11**, 11013 (2010).
- [10] H. Kobayashi, *Exp. Therm. Fluid Sci.* **26**, 375 (2002).
- [11] U. Frisch, in *Chaos and Statistical Methods*, edited by Y. Kuramoto (Springer, Berlin, 1984), p. 211.
- [12] D. Bessis and J. D. Fournier, *J. Phys. Lett.* **45**, L-833 (1984).
- [13] Z. Olami, B. Galanti, O. Kupervasser, and I. Procaccia, *Phys. Rev. E* **55**, 2649 (1997).
- [14] G. Joulin, *Combust. Sci. Technol.* **60**, 1 (1988).
- [15] R. V. Fursenko, K. L. Pan, and S. S. Minaev, *Phys. Rev. E* **78**, 056301 (2008).
- [16] V. Karlin, *Phys. Rev. E* **73**, 016305 (2006).
- [17] G. H. Markstein, *Nonsteady Flame Propagation* (Pergamon, Oxford, 1964).
- [18] A.-L. Barabasi and H. E. Stanley, *Fractal Concepts in Surface Growth* (Cambridge University Press, Cambridge, UK, 1995).
- [19] G. Joulin, *J. Phys. (France)* **50**, 1069 (1989).
- [20] B. Deconinck, Y. Kimura, and H. Segur, *J. Phys. A* **40**, 5459 (2007).
- [21] G. Joulin and B. Denet, *Phys. Rev. E* **78**, 016315 (2008).
- [22] Y. C. Lee and H. H. Chen, *Phys. Scr. T* **2**, 41 (1982).
- [23] M. L. Mehta, *Random Matrices*, 2nd ed. (Academic, Boston, 1991).
- [24] S. Gradshteyn and I. M. Ryzhik, *Tables of Integrals, Series and Products*, 7th ed. (Elsevier, Amsterdam, 2007).
- [25] Y. Chen and M. E. H. Ismail, *J. Phys. A* **31**, 5525 (1998).
- [26] Ya. B. Zel'dovich, A. G. Istratov, N. I. Kidin, and V. B. Librovich, *Combust. Sci. Technol.* **24**, 1 (1980).
- [27] G. E. Andrews, *The Theory of Partitions* (Cambridge University Press, Cambridge, 1984).
- [28] E. W. Weisstein, "Composition," From MathWorld, A Wolfram Web Resource [<http://mathworld.wolfram.com/Composition.html>].
- [29] M. E. H. Ismail, *Pacific J. Maths.* **193**, 355 (2000).
- [30] G. E. Andrews, R. Askey, and R. Roy, *Special Functions* (Cambridge University Press, Cambridge, 2000).
- [31] L. Guidi and D. Marchetti, *Phys. Lett. A* **308**, 162 (2003).
- [32] G. I. Sivashinsky, *Combust. Sci. Technol.* **62**, 77 (1988).
- [33] H. El-Rabii, G. Joulin, and K. A. Kazakov, *SIAM J. Appl. Math.* **70**, 3287 (2010).
- [34] F. A. Williams, in *Combustion Theory*, 2nd ed. (Benjamin/Cummings, Menlo Park, 1998), p. 389.
- [35] H. Kobayashi *et al.*, in *XXVIth International Symposium on Combustion* (The Combustion Institute, Pittsburgh, 1996), p. 389.